Improvement of a multigrid solver for 3D EM diffusion

T. Jönsthövel
Balijelaan 54 bis
3521 GV Utrecht

January 6, 2006

Contents

1 Abstract

Dit is eerste deel scriptie. Hoofdoel: introductie van het probleem met de MG solver. Het probleem uit de praktijk wordt overgeheveld naar een wiskundig model. Dit model resulteert in een formulering van de Maxwell vergelijkingen met PEC randvoorwaarden. Voor het oplossen van deze vergelijkingen wordt een MG methode gebruikt. Anisotropie door gridstretching levert problemen op in convergentiesnelheid en robuustheid. Dit verschijnsel kan (gedeeltelijk) verholpen worden door het gebruik van semicoarsening en een line-smoother. (Afmaken/aanpassen pas als thesis is voltooid)

2 Preface

In this thesis the first (X) chapters will present a detailed overview of the practical use of EM methods, the governing equations: the Maxwell equations, the discretization and the mathematical problems encountered by solving the resulting system of equations with a Multigrid solver. It has to be said that almost all of this pre-investigation has been done by Wim Mulder from Shell International Exploration and Production as it is his research this thesis will use as a starting point. However, in order to give the reader a clear view of the basics of the new research it is almost impossible to ignore the problem statement given as it is by Mulder. Therefore, the introduction of this thesis can be seen as a (sometimes) more extended version of Mulder's article concerning EM 3-D diffusion methods, 'a multigrid solver for 3-D electromagnetic diffusion'.

As stated above, the second part of this thesis will handle the improvements made on the Multigrid solver and the resulting mathematical implications. (*more text here when research/thesis is extended*)

3 Practical Problem/Application EM diffusion

3.1 Introduction EM methods

Electromagnetic methods (EM) have played a minor role in hydrocarbon exploration (oil/gas). Because EM methods use signals that diffuse in the Earth, they cannot provide the same vertical resolution as modern seismic exploration. Due

to improvements in magnetotelluric (MT) data collection, application of MT in settings where other exploration methods fail and MT being a complementary information source to seismic exploration, EM methods become more widely used in hydrocarbon exploration.

Just as in seismic exploration, EM methods can contribute to effective hydrocarbon exploration in two distinct ways:

1. Imaging structures that could host potential reservoirs and/or source rocks
2. Providing evidence for direct indication of the presence of hydrocarbons (e.g. the Troll field)

The table below summarizes the most common EM methods used in oil and gas exploration.

Method	Source	Signal type (freq or time domain)	Measured Fields (electric or Magnetic)	Depth of investigation in a sedimentary basin	Land or marine
MT	Natural	Frequency	E and H	1 – 10 km	Both
AMT (audio MT)	Natural	Frequency	E and H	100 – 1000 m	Land
CSAMT (controlled source audio MT)	Grounded Dipole	Frequency	E and H	100 – 2000 m	Both

Next a review of an arbitrary EM method is presented which can be used in seabottom exploration.

3.2 Basics EM diffusion

Consider the next situation. Suppose there is an indication that there might be a reservoir of an unknown liquid or gas in the bottom, as drawn in the figure below:

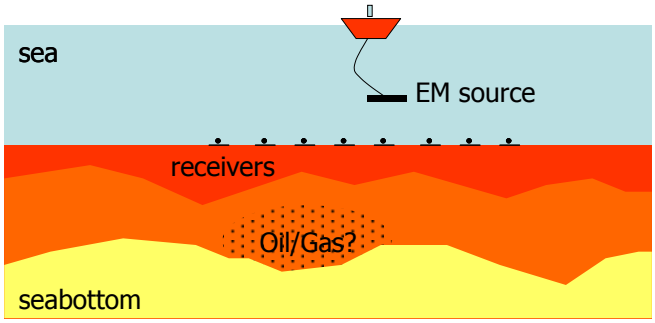

At the surface between sea and seabottom, a large number of receivers is placed. Next, a ship with a large cable, which *works* as an EM source, sails above the receivers.

The EM waves coming from the source, with frequencies in the band 10^3-10^{-4} Hz, travel through the water and diffuse into the earth and attenuate rapidly with depth. The penetration depth is called the skip depth. The surface measurement of electric and magnetic fields at the receivers gives the average resistivity from the surface to a depth equivalent of the skin depth. The skin depth increases as frequency decreases, and therefore a resistivity profile of the seabottom can be achieved by recording a range of frequencies. However, the seawater in deep oceans, a major conductor, screens out high frequency signals (above 10^{-2} Hz) needed to image structure in the upper few kilometers of the seabottom. But with modern recording equipment in low noise environments, higher frequency signals can be detected in moderate water depths.

For example a resistivity model from Xiao and Unsworth (2004) derived by 2D inversion of the University of Alberta MT profile using the algorithm of Rodi and Mackie (2001). The black triangles show locations where MT data was recorded:

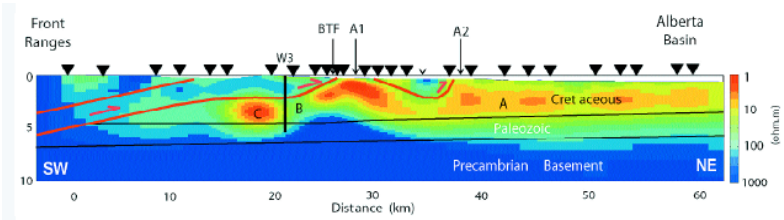

4 Maxwell equations

Changes in the electromagneticfield described in the previous chapter are governed by the Maxwell equations. Later on it becomes clear that these equations are the basis for the EM diffusion method.

The Maxwell equations (ME) are the set of four fundamental equations governing electromagnetism, i.e. the behavior of electric and magnetic fields. For time-varying fields, the differential form of these equations is:

$$\begin{aligned} &\nabla \times \mathbf{E} + \partial_t \mathbf{B} = 0 \quad \text{(Faraday's law)} \\ &\nabla \times \mathbf{H} - \partial_t \mathbf{D} = J \quad \text{(Maxwell-Ampère law)} \\ &\nabla \cdot \mathbf{D} = \rho_e \\ &\nabla \cdot \mathbf{B} = 0 \end{aligned} \tag{1}$$

The quantities above are functions of space $\mathbf{x}$ and time t. The vector fields are $\mathbf{E}$ (the electric field), $\mathbf{H}$ (the magnetic field), $\mathbf{D}$ (the electric displacement) and $\mathbf{B}$ (the magnetic induction). The scalars are $\mathbf{J}$ (the electric current density) and ρ_e (the electric charge density).

The equations from (1) form an underdetermined system (Aruliah, ?). A determinate system requires further assumptions. Hence, impose constitutive

relations between the field quantities in order to make the system (1) definite. These take the form:

$$\begin{aligned} \mathbf{D} &= \epsilon\mathbf{E} \\ \mathbf{B} &= \mu\mathbf{H} \\ \mathbf{J} &= \sigma\mathbf{E} + \mathbf{J}_s \end{aligned}$$

Where ϵ is the electric permittivity, μ is the magnetic permeability and σ is the conductivity of the media in which the electromagnetic field exists. Notify that $\sigma\mathbf{E}$ is in fact Ohm's law and $\mathbf{J}_s$ is the current density due to an external applied electric source (e.g. the cable under the ship, Chapter 1.2).

In free space, ϵ and μ are isotropic and homogeneous. The corresponding permittivity of free space is constant and denoted ϵ_0 while the permeability of free space is also constant and denoted μ_0. Free space is nonconductive so $\sigma = 0$. In this situation an exact solution of the Maxwell equations can be determined. However, for more realistic problems, like geophysical data inversion, the material properties are usually not homogeneous and have discontinuities across the material boundaries (e.g. air and sea, sea and bottom).

Choose E and H as the unknown fields, Maxwell equations now become:

$$\begin{aligned} &\nabla \times \mathbf{E} + \mu\partial_t\mathbf{H} = 0 \\ &\nabla \times \mathbf{H} - \sigma\mathbf{E} - \epsilon\partial_t\mathbf{E} = \mathbf{J}_s \\ &\nabla \cdot (\epsilon\mathbf{E}) = \rho_e \\ &\nabla \cdot (\mu\mathbf{H}) = 0 \end{aligned} \tag{2}$$

In this particular case, ϵ and μ are assumed to be constant and can be written as: $\epsilon = \epsilon_r\epsilon_0$ and $\mu = \mu_r\mu_0$. Where, ϵ_r is the relative permittivity and ϵ_0 the vacuum value. Similarly, μ_r is the relative permeability and μ_0 the vacuum value. Also, the last two Maxwell equations are not taken into account as they are of no importance for this EM method (*further investigation has to be done here*).

The magnetic field can be eliminated from (2):

$$\begin{array}{lcl} \nabla \times \mathbf{E} + \mu\partial_t\mathbf{H} = 0 & \Longleftrightarrow & -\mu^{-1}\nabla \times \mathbf{E} = \partial_t\mathbf{H} \\ \nabla \times \mathbf{H} - \sigma\mathbf{E} - \epsilon\partial_t\mathbf{E} = \mathbf{J}_s & \Longleftrightarrow & \nabla \times \partial_t\mathbf{H} - \sigma\partial_t\mathbf{E} - \epsilon\partial_{tt}\mathbf{E} = \partial_t\mathbf{J}_s \\ & \Downarrow & \\ & \nabla \times \mu^{-1}\nabla \times \mathbf{E} + \sigma\partial_t\mathbf{E} + \epsilon\partial_{tt}\mathbf{E} = -\partial_t\mathbf{J}_s & \end{array}$$

As described in Chapter 1 most electromagnetic fields are in the frequency domain. Also to avoid the use of an implicit (more difficult) time-stepping scheme, a transformation from the time to the frequency domain is introduced. Consider the following Fourier transformation:

$$\mathbf{E}(\mathbf{x}, t) = \frac{1}{2\pi}\int_{-\infty}^{\infty} \hat{\mathbf{E}}(\mathbf{x}, \omega)\, e^{-i\omega t} d\omega$$

Suppose $F_{x,t}\left(f(x,t)\right)(\omega)$ is the fouriertransform of $f(x,t)$ then for the n^{th} derivative this yields:

$$\mathcal{F}_{\mathbf{x},t}\left[f^{(n)}\left(\mathbf{x},t\right)\right](\omega) = (i\omega)^n \mathcal{F}_{\mathbf{x},t}\left[f\left(\mathbf{x},t\right)\right](\omega)$$

Therefore the following equation is obtained:

$$i\omega\mu_0\tilde{\sigma}\hat{\mathbf{E}} - \nabla \times \mu_r^{-1}\nabla \times \mathbf{E} = -i\omega\mu_0\mathbf{J}_s \tag{3}$$

Where, $\tilde{\sigma}(\mathbf{x}) = \sigma - i\omega\epsilon$ is the complex conductivity. Usually, $|\omega\epsilon| \ll \sigma$. From now, $\hat{\mathbf{E}}$ will be written as $\mathbf{E}$ for convenience. On the boundaries of all domains introduced in the following chapters, perfectly electrically conducting (PEC) boundary conditions will be used:

$$\mathbf{n} \times \mathbf{E} = 0 \text{ and } \mathbf{n} \cdot \mathbf{H} = 0$$

Here, $\mathbf{n}$ is the outward normal on the boundary of the domain.

5 Discretization equations

Equation (3) can be discretized by the Finite Integration technique (FIT) (Clemens & Weiland, 2001). This scheme can be viewed as a finite-volume generalization of Yee's scheme (Yee, 1966) for tensor-product Cartesian grids with variable grid spacings. An error analysis has been made for the constant-coefficient case (Monk & Süli, 1994) and both the electric and magnetic field components appear to have second-order accuracy. (Mulder, 2005)

Introduce a tensor-product grid with nodes at positions (x_k, y_l, z_m) with $k = 0...N_x$, $l = 0...N_y$ and $m = 0...N_z$. Note that N_x, N_y and N_z are odd, integers and can be described as: $N_i = 2^{m_i} + 1$. The grid contains $N_x \times N_y \times N_z$ cells with these nodes as vertices. The cell centres are located at:

$$\begin{aligned} x_{k+\frac{1}{2}} &= \frac{1}{2}\left(x_k + x_{k+1}\right) \\ y_{l+\frac{1}{2}} &= \frac{1}{2}\left(y_l + y_{l+1}\right) \\ z_{m+\frac{1}{2}} &= \frac{1}{2}\left(z_m + z_{m+1}\right) \end{aligned}$$

Analogue to Yee's scheme, the electric field components are located at positioned at the edges of the cells and the magnetic field components are located at the middle of the faces of the cell:

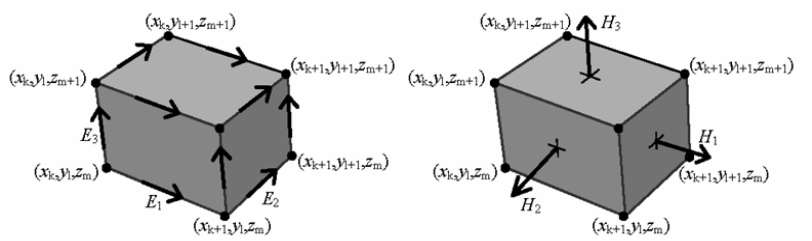

Now, the component of the electricfield $E_{1,k+\frac{1}{2},l,m}$ represents the average of $E_1(x, y_l, z_m)$ over the edge from x_k to x_{k+1} at given y_l and z_l. This can be written as:

$$E_1(x_{k+\frac{1}{2}}, y_l) = \frac{1}{x_{k+1} - x_k} \int_{x_k}^{x_{k+1}} E_1(x, y_l, z_m) dx$$

Other components of the electricfield are defined in a similar way. The material properties, $\tilde{\sigma}$ and μ_r^{-1} are assumed to be given as cell-averaged values.

Next, each part of equation (3) will be discretized First, dual volumes related to the edges are introduced. For a given edge, the dual volume is the sum of the quarters of the total volume of the four neighboring cells:

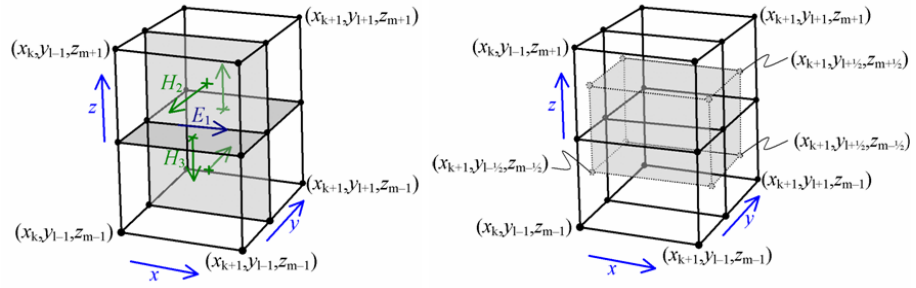

The volume of a normal cell is defined as:

$$V_{k+\frac{1}{2},l+\frac{1}{2},m+\frac{1}{2}} = h^x_{k+\frac{1}{2}} h^y_{l+\frac{1}{2}} h^z_{m+\frac{1}{2}}$$

With,

$$\begin{aligned} h^x_{k+\frac{1}{2}} &= x_{k+1} - x_k \\ h^y_{l+\frac{1}{2}} &= y_{l+1} - y_l \\ h^z_{m+\frac{1}{2}} &= z_{m+1} - z_m \end{aligned}$$

The dual volume of the edge on which $E_{1,k+\frac{1}{2},l,m}$ lives:

$$V_{k+\frac{1}{2},l,m} = \frac{1}{4} h^x_{k+\frac{1}{2}} \sum_{m_2=0}^{1} \sum_{m_3=0}^{1} h^y_{l-\frac{1}{2}+m_2} h^z_{m-\frac{1}{2}+m_3}$$

Where,

$$\begin{aligned} d^x_k &= x_{k+\frac{1}{2}} - x_{k-\frac{1}{2}} \\ d^y_l &= y_{l+\frac{1}{2}} - y_{l-\frac{1}{2}} \\ d^z_m &= z_{m+\frac{1}{2}} - z_{m-\frac{1}{2}} \end{aligned}$$

So,

$$\begin{aligned} V_{k+\frac{1}{2},l,m} &= h^x_{k+\frac{1}{2}} d^y_l d^z_m \\ V_{k,l+\frac{1}{2},m} &= h^y_{l+\frac{1}{2}} d^x_k d^z_m \\ V_{k,l,m+\frac{1}{2}} &= h^z_{m+\frac{1}{2}} d^x_k d^y_l \end{aligned}$$

Note that d^x_k, d^y_l and d^z_m are not defined at the boundaries yet. There are two options. First, take $d^x_0 = h^x_{\frac{1}{2}}$ at $k = 0$ and $d^x_{N_X} = h^x_{N_X-\frac{1}{2}}$ at $k = N_x$, repeat for other directions. Or secondly, use Monk & Süli, $d^x_0 = \frac{1}{2} h^x_{\frac{1}{2}}$ at $k = 0$ and $d^x_{N_X} = \frac{1}{2} h^x_{N_X-\frac{1}{2}}$ at $k = N_x$.

The discretization of (3):

1. $i\omega\mu_0\tilde{\sigma}E$

   The discrete form of this term multiplied by the corresponding dual volume (Finite Integration Technique) becomes $S_{k+\frac{1}{2},l,m} E_{1,k+\frac{1}{2},l,m}$, $S_{k,l+\frac{1}{2},m} E_{2,k,+\frac{1}{2}l,m}$, $S_{k,l,m+\frac{1}{2}} E_{3,k,l,m+\frac{1}{2}}$ for the first, second and third component respectively. Here $S = i\omega\mu_0\tilde{\sigma}V$ is defined in terms of cell-averages.

   e.g. The coefficient for $E_{1,k+\frac{1}{2},l,m}$ becomes:

$$\begin{aligned} S_{k+\frac{1}{2},l,m} &= \frac{1}{4}(S_{k+\frac{1}{2},l-\frac{1}{2},m-\frac{1}{2}} + S_{k+\frac{1}{2},l+\frac{1}{2},m-\frac{1}{2}} \\ &\quad + S_{k+\frac{1}{2},l-\frac{1}{2},m+\frac{1}{2}} + S_{k+\frac{1}{2},l+\frac{1}{2},m+\frac{1}{2}}) \end{aligned}$$

2. $\nabla \times \mu_r^{-1} \nabla \times E$

   The discretization of this term is not straightforward. First, the curl of the electricfield components is discretized and placed at the middle of the faces of the grid cells. When divided by $i\omega\mu$, these are in fact the components of the magneticfield (see figure MULDER) that are normal to the face of the cell. Next, the curl of the discretized components is again discretized in a similar way.

(a) $\mathbf{v} = \nabla \times E$

The curl of E can be discretized with Stokes's theorem (Adams, 2000):

$$\oint_C E \cdot d\mathbf{r} = \int_V (\nabla \times E) \cdot \mathbf{n} dV$$

Now consider the grid cell in figure (MULDER). First, apply Stokes's Theorem at components E_1 and E_3 lying at edge of the surface $[x_k, x_{k+1}] \times [z_m, z_{m+1}]$. In detail:

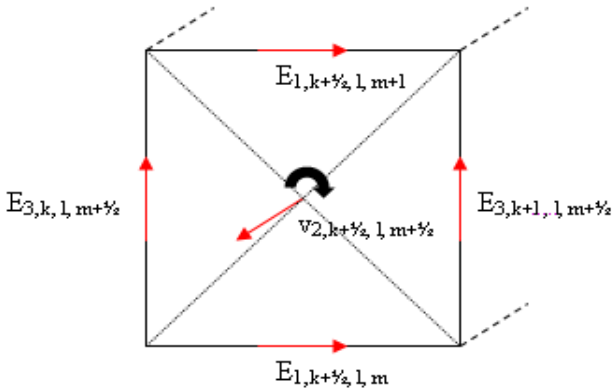

In continuous form with $\mathbf{n}$ the outward normal of the grid cell,

$$\oint_C E \cdot d\mathbf{r} = \oint_C E_1(x,y,z)dx + E_2(x,y,z)dy = \int_V (\nabla \times E) \cdot \mathbf{n} dV$$

In discrete form,

$$\begin{aligned} & \left(E_3(x_k, y_l, z_{m+\frac{1}{2}})h^z_{m+\frac{1}{2}} + E_1(x_{k+\frac{1}{2}}, y_l, z_{m+1})h^x_{k+\frac{1}{2}}\right) \\ & - \left(E_3(x_{k+1}, y_l, z_{m+\frac{1}{2}})h^z_{m+\frac{1}{2}} + E_1(x_{k+\frac{1}{2}}, y_l, z_m)h^x_{k+\frac{1}{2}}\right) \\ = \; & V \cdot (\nabla \times E) \begin{pmatrix} 0 & 1 & 0 \end{pmatrix}^{\mathbf{T}} = V \cdot v_2(x_{k+\frac{1}{2}}, y_l, z_{m+\frac{1}{2}}) \\ = \; & h^z_{m+\frac{1}{2}} h^x_{k+\frac{1}{2}} \cdot v_2(x_{k+\frac{1}{2}}, y_l, z_{m+\frac{1}{2}}) \end{aligned}$$

Note that the path integral follows the direction of the curl operator and therefore two electricfield components ($E_{1,k+\frac{1}{2},l,m}$ and $E_{3,k+1,l,m+\frac{1}{2}}$) point in the opposite direction.
Simplify,

$$\begin{aligned} v_{2,k+\frac{1}{2},l,m+\frac{1}{2}} \; = \; & \frac{1}{h^x_{k+\frac{1}{2}}} \left(E_3(x_k, y_l, z_{m+\frac{1}{2}}) - E_3(x_{k+1}, y_l, z_{m+\frac{1}{2}})\right) \\ & - \frac{1}{h^z_{m+\frac{1}{2}}} \left(E_1(x_{k+\frac{1}{2}}, y_l, z_{m+1}) - E_1(x_{k+\frac{1}{2}}, y_l, z_{m+1})\right) \end{aligned}$$

Repeat this procedure two gain the two remaining discretized curl components v_1 and v_2:

$$\begin{aligned} v_{1,k,l+\frac{1}{2},m+\frac{1}{2}} &= \frac{1}{h^y_{l+\frac{1}{2}}}\Big(E_3(x_k, y_{\,l+1}, z_{m+\frac{1}{2}}) - E_3(x_k, y_{\,l}, z_{m+\frac{1}{2}})\Big) \\ &\quad -\frac{1}{h^z_{m+\frac{1}{2}}}\Big(E_1(x_k, y_{\,l+\frac{1}{2}}, z_{m+1}) - E_1(x_k, y_{\,l+\frac{1}{2}}, z_m)\Big) \end{aligned}$$

$$\begin{aligned} v_{3,k+\frac{1}{2},l,m+\frac{1}{2}} &= \frac{1}{h^x_{k+\frac{1}{2}}}\Big(E_2(x_{k+1}, y_{\,l+\frac{1}{2}}, z_m) - E_2(x_k, y_{\,l+\frac{1}{2}}, z_m)\Big) \\ &\quad -\frac{1}{h^y_{l+\frac{1}{2}}}\Big(E_1(x_{k+\frac{1}{2}}, y_{\,l+1}, z_m) - E_1(x_{k+\frac{1}{2}}, y_{\,l}, z_m)\Big) \end{aligned}$$

(b) $\mu_r^{-1}\nabla \times E$

The scaling by μ_r^{-1} at the face requires another averaging procedure because the material properties are assumed to be given as cell-averaged values:

$$\iiint_V \mu_r^{-1} dV = V\mu_r^{-1}$$

Hence, define $M = V\mu_r^{-1}$:

$$M_{k+\frac{1}{2},l+\frac{1}{2},m+\frac{1}{2}} = h^x_{k+\frac{1}{2}} h^y_{l+\frac{1}{2}} h^z_{m+\frac{1}{2}} \mu^{-1}_{r,k+\frac{1}{2},l+\frac{1}{2},m+\frac{1}{2}}$$

for a given cell $(k+\frac{1}{2}, l+\frac{1}{2}, m+\frac{1}{2})$. So, an averaging step in the z-direction provides:

$$M_{k+\frac{1}{2},l+\frac{1}{2},m} = \frac{1}{2}\Big(M_{k+\frac{1}{2},l+\frac{1}{2},m-\frac{1}{2}} + M_{k+\frac{1}{2},l+\frac{1}{2},m+\frac{1}{2}}\Big)$$

at the face $(k+\frac{1}{2}, l+\frac{1}{2}, m)$ between the cells $(k+\frac{1}{2}, l+\frac{1}{2}, m+\frac{1}{2})$ and $(k+\frac{1}{2}, l+\frac{1}{2}, m-\frac{1}{2})$.

In the previous step the curl of E has been discretized. Now multiply with the discrete factor $\mu_r^{-1}V$:

$$\begin{aligned} u_{1,k,l+\frac{1}{2},m+\frac{1}{2}} &= M_{k,l+\frac{1}{2},m+\frac{1}{2}} v_{1,k,l+\frac{1}{2},m+\frac{1}{2}} \\ u_{2,k+\frac{1}{2},l,m+\frac{1}{2}} &= M_{k+\frac{1}{2},l,m+\frac{1}{2}} v_{2,k+\frac{1}{2},l,m+\frac{1}{2}} \\ u_{3,k+\frac{1}{2},l,m+\frac{1}{2}} &= M_{k+\frac{1}{2},l,m+\frac{1}{2}} v_{3,k+\frac{1}{2},l,m+\frac{1}{2}} \end{aligned}$$

(c) $\nabla \times \mu_r^{-1} \nabla \times E$

At last, only $\nabla \times \mathbf{u}$ has to be discretized. Note that the components of $\mathbf{u}$ are related to the magnetic field components by:

$$\begin{aligned} u_{1,k,l+\frac{1}{2},m+\frac{1}{2}} &= i\omega\mu_0 V_{k,l+\frac{1}{2},m+\frac{1}{2}} H_{1,k,l+\frac{1}{2},m+\frac{1}{2}} \\ u_{2,k+\frac{1}{2},l,m+\frac{1}{2}} &= i\omega\mu_0 V_{k+\frac{1}{2},l,m+\frac{1}{2}} H_{2,k+\frac{1}{2},l,m+\frac{1}{2}} \\ u_{3,k+\frac{1}{2},l,m+\frac{1}{2}} &= i\omega\mu_0 V_{k+\frac{1}{2},l,m+\frac{1}{2}} H_{3,k+\frac{1}{2},l,m+\frac{1}{2}} \end{aligned}$$

where,

$$\begin{aligned} V_{k,l+\frac{1}{2},m+\frac{1}{2}} &= d_k^x h_{l+\frac{1}{2}}^y h_{m+\frac{1}{2}}^z \\ V_{k+\frac{1}{2},l,m+\frac{1}{2}} &= h_{k+\frac{1}{2}}^x d_l^y h_{m+\frac{1}{2}}^z \\ V_{k+\frac{1}{2},l,m+\frac{1}{2}} &= h_{k+\frac{1}{2}}^x h_{l+\frac{1}{2}}^y d_m^z \end{aligned}$$

The components of $\mathbf{u}$ lie on the edges of the dual volumes as introduced earlier:

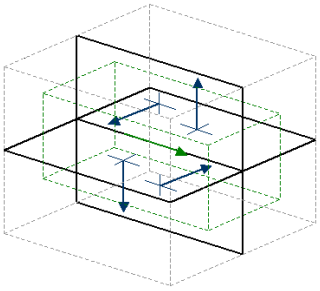

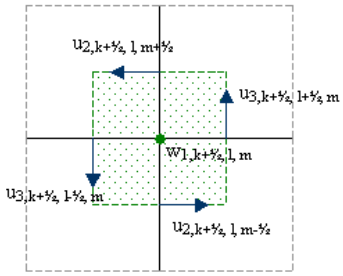

The first component of the curl, w_1, is evaluated by applying Stokes's Theorem again:

$$\oint_C E \cdot d\mathbf{r} = \int_V (\nabla \times E) \cdot \mathbf{n} dV$$

With C a rectangle of the dual volume that is obtained for constant x and V the volume of the dualvolume.

2. $i\omega\mu_0 \mathbf{J}_s$

(a) The discretization of the source term is straightforward:

$$\begin{aligned} s_{1,k+\frac{1}{2},l,m} &= i\omega\mu_0 V_{k+\frac{1}{2},l,m} J_{1,k+\frac{1}{2},l,m} \\ s_{2,k,l,m+\frac{1}{2}} &= i\omega\mu_0 V_{k,l+\frac{1}{2},m} J_{2,k,l,m+\frac{1}{2}} \\ s_{3,k,l,m+\frac{1}{2}} &= i\omega\mu_0 V_{k,l,m+\frac{1}{2}} J_{3,k,l,m+\frac{1}{2}} \end{aligned}$$

Let the residual for an arbitrary electric field that is not necessarily a solution to the problem, be defined as:

$$\mathbf{r} = V\left(i\omega\mu_0\tilde{\sigma}\hat{\mathbf{E}} - \nabla\times\mu_r^{-1}\nabla\times\mathbf{E} + i\omega\mu_0\mathbf{J}_s\right)$$

In discrete form:

$$\begin{aligned} r_{1,k+\frac{1}{2},l,m} &= s_{1,k+\frac{1}{2},l,m} + S_{k+\frac{1}{2},l,m}E_{1,k+\frac{1}{2},l,m} \\ &\quad - \left[e^y_{l+\frac{1}{2}}u_{3,k+\frac{1}{2},l+\frac{1}{2},m} - e^y_{l-\frac{1}{2}}u_{3,k+\frac{1}{2},l-\frac{1}{2},m}\right] \\ &\quad + \left[e^z_{m+\frac{1}{2}}u_{2,k+\frac{1}{2},l,m+\frac{1}{2}} - e^z_{m-\frac{1}{2}}u_{2,k+\frac{1}{2},l,m-\frac{1}{2}}\right] \end{aligned}$$

$$\begin{aligned} r_{2,k,l+\frac{1}{2},m} &= s_{2,k,l+\frac{1}{2},m} + S_{k,l+\frac{1}{2},m}E_{2,k,l+\frac{1}{2},m} \\ &\quad - \left[e^z_{m+\frac{1}{2}}u_{1,k,l+\frac{1}{2},m+\frac{1}{2}} - e^z_{m-\frac{1}{2}}u_{1,k,l+\frac{1}{2},m-\frac{1}{2}}\right] \\ &\quad + \left[e^x_{k+\frac{1}{2}}u_{3,k+\frac{1}{2},l+\frac{1}{2},m} - e^x_{k-\frac{1}{2}}u_{3,k-\frac{1}{2},l+\frac{1}{2},m}\right] \end{aligned}$$

$$\begin{aligned} r_{3,k,l,m+\frac{1}{2}} &= s_{3,k,l,m+\frac{1}{2}} + S_{k,l,m+\frac{1}{2}}E_{3,k,l,m+\frac{1}{2}} \\ &\quad - \left[e^x_{k+\frac{1}{2}}u_{2,k+\frac{1}{2},l,m+\frac{1}{2}} - e^x_{k-\frac{1}{2}}u_{2,k-\frac{1}{2},l,m+\frac{1}{2}}\right] \\ &\quad + \left[e^y_{l+\frac{1}{2}}u_{1,k,l+\frac{1}{2},m+\frac{1}{2}} - e^y_{l-\frac{1}{2}}u_{1,k,l-\frac{1}{2},m+\frac{1}{2}}\right] \end{aligned}$$

It may appear that the weighting of the differences is in contradiction with Stokes's theorem as stated above in step 2c. However, the differences have been multiplied by the local dual volume.

The discretization has been completed. The next step is to find the solution $\mathbf{E}$ of $\mathbf{r} = 0$ for a given domain, material parameters, source term and boundary conditions.

6 Multigrid solver

In this chapter a brief summary of the basic principles of multigrid is given. At the end of this chapter a description of the different multigridcomponents used by Mulder can be found.

6.1 Basics Multigrid (two-grid)

Consider the following discretization of an arbitrary equation on a grid with spatial mesh size h, Ω_h:

$$A_h x_h = b_h$$

If the solution of this equation is approximated by x_h^m, the residual and error are as follows:

$$\begin{aligned} e_h^m &: = x_h - x_h^m \\ r_h^m &: = b_h - A_h x_h^m \end{aligned}$$

This results in the defect equation which is equivalent with the original equation because $x_h = x_h^m + e_h^m$:

$$A_h e_h^m = r_h^m$$

If a basic iterative method, like Jacobi or Gauss-Seidel, is used to solve the equation and the error is computed then it appears that the error becomes smooth after several iteration steps. In that case the iteration formula can be interpreted as an error averaging process. This error-smoothing is one of the two basic principles of the multigrid approach. The other principle is based on the fact that a quantity that is smooth on a certain grid can also be approximated on a coarser grid. So if the error of the approximation of the solution has become smooth after several relaxation sweeps, then this error can be approximated with a suitable procedure on a coarser grid.

Suppose that the matrix A_h can be approximated by a more manageable matrix $\hat{A}_h$ then:

$$\hat{A}_h \hat{e}_h^m = r_h^m \longrightarrow x_h^{m+1} = x_h^m + \hat{e}_h^m$$

The idea of multigrid is to approximately solve the defect equation on a coarser grid with spatial mesh size, e.g. $H := 2h$. Obviously, this will take less time and work than a conventional direct method.

$$A_H \hat{e}_H^m = r_H^m$$

Assume that A_H^{-1} exists. As r_H^m and $\hat{e}_H^m$ are grid functions on the coarser grid, introduce two (linear) transfer operators:

$$I_h^H : \mathcal{G}(\Omega_h) \longrightarrow \mathcal{G}(\Omega_H),\ I_H^h : \mathcal{G}(\Omega_H) \longrightarrow \mathcal{G}(\Omega_h)$$

These functions are necessary to restrict and prolongate the residuals and approximations of the error to different coarser and finer grids. This yields,

$$\begin{aligned} r_H^m &: = I_h^H r_h^m, \text{ restrict } r_h^m \text{ to } \Omega_H \\ \hat{e}_h^m &: = I_H^h \hat{e}_H^m, \text{ prolongate } \hat{e}_H^m \text{ to } \Omega_h \end{aligned}$$

One choice can be the injection operator. For instance, the residual on a coarse grid Ω_H will be mapped directly to the finer grid Ω_h. No weighting has been applied. Other operators are based on (full) weighting and linear or bilinear interpolation. The next section will provide more insight.

Unfortunately coarse grid correction alone is not enough. In general, the interpolation of coarse grid corrections reintroduces high frequency error components on the fine grid (Oosterlee, 200?). One natural approach to reduce them is to introduce one or a few additional smoothing sweeps after the coarse grid correction. These sweeps are known as pre- and post-smoothing.

6.1.1 Multigrid cycle

Together the different multigrid components pre-smoothing, coarse grid correction and post-smoothing form one multigrid cycle. In the Appendix (??) an overview of a general multigridcycle can be found.

If multigrid is applied recursively, a strategy is required for moving through the various grids. Several possibilities are the V-cycle, W-cycle and F-cycle. The main differences between these approaches are the number of pre- and post-smoothing steps and the different number of coarser grids used. However, through trial and error the F-cycle has proven itself as a relative low-cost and reliable multigrid cycle for this particular case (Maxwell equations). Therefore, the other cycles are not taken into account throughout the rest of this thesis.

One reason why multigrid methods may fail to converge is strong anisotropy in the coefficients of the governing equation. In that case more sophisticated smoothers or coarsening strategies may be required. If slow convergence is caused by just a few components of the solution, a Krylov subspace method can be used to effectively remove them. In this particular case the matrix A is non-symmetric and complex. Therefore BiCGstab (Van der Vorst, 1992) is a suitable alternative. Multigrid will be accelerated by the Krylov method. Alternatively, the multigrid can also be seen as a preconditioner for BiCGstab.

6.2 Multigrid Components Mulder

As described above, the following multigrid components have to be defined:

- Coarse grid specification
- Smoother
- Restriction operator
- Prolongation operator

In Feigh et al. (2003) a multigrid method for a FIT discretization has been presented. Mulder uses this approach as a starting point and adapts some components of the multigrid solver.

6.2.1 Coarse grid specification

The FIT discretization uses a tensor-product Cartesian grid. The coarse-grid cells are formed by combining 2x2x2 fine-grid cells, this is a special case of the method in Feigh et al (2003) where arbitrary coarser-grids are used with nodes that are not necessarily a subset of those on the fine grid. Obvious, in this case the coarse-grid nodes are a subset of the fine-grid nodes. For example, consider the very simplified 2-D situation below:

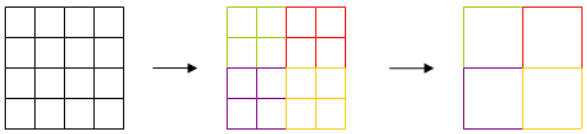

(4)

The fine grid with 4x4 cells maps to a coarser-grid with 2x2 cells. Four neighboring fine grid cells are put together in order to form one coarser-grid cell. This example can easily be extended to three dimensions and a more sophisticated (stretched) tensor-product Cartesian grid.

6.2.2 Smoother

The smoother has to vital tasks. First, of course, it acts as a smoother. The high-frequency error components on the fine grids are smoothed down. Secondly, it computes locally a new approximation for the solution x_H of $A_H x_H = b_H$, with H the coarsest spatial mesh size.

As smoother the method proposed by Arnold et al (2000) is used. This smoother has the nice property that it automatically imposes the divergence-free character of $\tilde{\sigma}\mathbf{E}$ and does not require an explicit divergence correction as in Hiptmair (1998).

The method selects one node and solves for the six degrees of freedom on the six edges attached to the node. The smoother is applied in a symmetric Gauss-Seidel fashion, following the lexicographical ordering of the nodes (x_k, y_l, z_m). This means that the index goes from (x_1, y_1, z_1) to (x_{Nx}, y_1, z_1) and then from (x_1, y_2, z_1) to (x_{Nx}, y_2, z_1) etc. Due to the PEC boundary conditions the system of equations of the nodes on the boundary have not to be solved because the solution of the electricfield components is already known there.

After each node is done, the electricfield components are updated with the most recent solution. When the first smoothing step is finished the next one is carried out in opposite direction. So, the index starts with (x_{Nx}, y_{Ny}, z_{Nz}) and follows it's way in a lexicographical order back to (x_1, y_1, z_1).

. When this smoother is applied to equation (3), a 6x6 system of equations has to be solved locally. Suppose a node at position (x_k, y_l, z_m) has been selected:

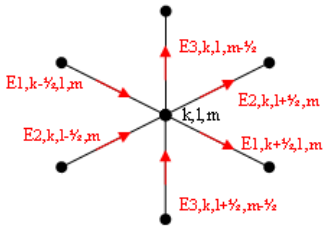

This yields the following (local) system of equations

$$AE_{k,l,m} = -(s + BE_{sur}) \tag{5}$$

Where, $E_{k,l,m}$ is a vector containing the six electricfield components lying at the surrounding edges of the node. Matrix A contains all the coefficients belonging to six entries of the vector $E_{k,l,m}$. The vector s contains the six corresponding source terms (see equation 3) and the vector resulting from the matrix-vector multiplication BE_{sur}, contains all information from surrounding electricfield components. The latter have to be taken into account because they are needed to compute the curl operator of equation (3). Consider figure below:

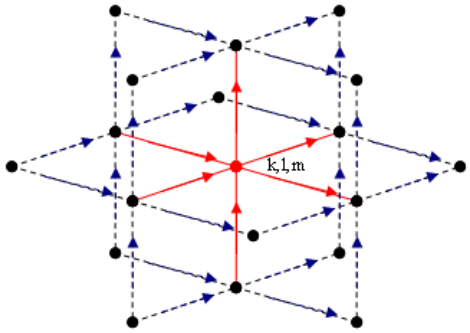

The red arrows represent the six unknown electricfield components lying on the edges and surrounding grid node (x_k, y_l, z_m). The 24 blue arrows are the electricfield components corresponding to neighboring grid nodes which are needed to compute the discretization of the curl operator lying on the same edges as the entries of $E_{k,l,m}$. All matrices and vectors of (5) are described in detail and can be found in Appendix (??).

The question remains when this smoother is applied? One full multigridcycle contains two post-smoothing steps ($v_2 = 2$, see multigridcycle Appendix) which is equivalent with one symmetric Gauss-Seidel iteration. Furthermore, pre-smoothing has not been applied ($v_1 = 0$) and other choices have not been studied here.

There is one remark. In the case that $\tilde{\sigma} = 0$, which may occur if the electricfield in air is modelled and ϵ_r is set to zero, the local 6x6 systems become

singular. This problem can be (artificially) avoided when solving the small local systems by replacing $\tilde{\sigma}$ with a small positive number.

6.2.3 Restriction Operator

In this section the restriction operator will be described.

Suppose for simplicity that $N_x = N_y = N_z = 2^m + 1$, with integer $m \geq 1$. The coarse grid is defined as above (Coarse grid specification).
The discrete operator on the coarser grids is chosen to be the same as the one obtained by direct discretization. The cell-averaged material properties are obtained from the finer grids by summing the values of S and M of the fine-grid cells lying inside a coarser-grid cell. The coarsest grid has 2x2x2 grid cells. Here, the smoother acts as a direct solver.
When normal coarsening is applied the following situation occurs:

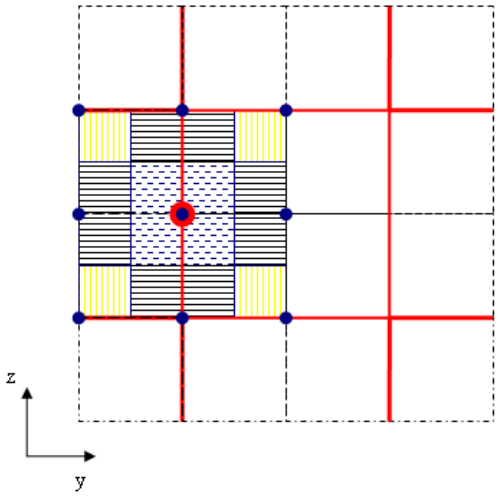

The figure shows the grid from besides, the x-direction is perpendicular to the paper. The blue dots represent the coarse grid electricfield components, E_1, lying at the edges of the grid cells. The red dot in the middle represents the fine grid electricfield component E_1. The thick red lines are the edges of the coarse grid cells, whereas the black lines represent the edges of the fine grid cells.
The idea behind the restriction of the fine grid components to coarse grid components is that the calculation of the coarse grid electricfield components is in fact a weighted summation of surrounding fine grid electricfield components. Each fine grid electricfield component is multiplied with a weighting factor and than the values all of 18 surrounding components are summed up to become the value of one coarse grid electricfield component. The question remains, how to determine the weighting factors?
Remember that in previous sections the dualvolumes were introduced. These

volumes determine how much a fine-grid electricfield component should be taken into account when restricting to a coarser grid. In the figure above, the yellow and blue striped rectangles represent the parts of the dual volumes of the fine grid electricfield components which lie in the dualvolume of the coarse-grid electricfield component. The weighting factor for each blue dot is the quotient of how much of the dualvolume lies in the coarse-grid dualvolume and the complete dualvolume of this fine-grid electricfield component. One can see and easily deduce that for the blue dots above this will be factors $\frac{1}{8}$,$\frac{1}{4}$, $\frac{1}{2}$ and 1.

It should be noted that this restriction operator is second order accurate (exact for linear functions in a pointwise sense) on equidistant grids, but only first-order accurate on stretched grids. Another, more simple, choice can be made for this restriction operator. However, numerical experiments on stretched grids showed that this choice led to divergence in some cases.

6.2.4 Prolongation

After computing the exact of approximate solution of the discrete equations on the coarse grids, the solution needs to be interpolated back to the fine grid and added to the fine-grid solution. A natural prolongation operator is the rescaled transpose of the restriction operator. This means that the same weights as above are applied for the electricfield components. This operator is identical to constant interpolation in the coordinate direction of the component and bilinear interpolation for the other coordinates.

In practice, this can be done with a matlab procedure `interpn` which can perform linear interpolations.

7 Overview problems Multigrid

In this chapter a short summary is given of the problems encountered by Mulder in the performance of the multigridsolver. First a testproblem will be introduced. This problem is defined by Mulder and based on an approach which can be found in Aruliah et al (2001). With this test case the multigrid solver of Mulder has been tested. Problems which did arise from other test cases done by Mulder are listed at the end of this chapter.

7.1 Testproblem: eigenvalues

This testproblem is based on eigenfunctions and first introduced in Aruliah et al (2001). It has been modified by mulder to allow for the use of perfectly conduction (PEC) boundary conditions. The domain is $\Omega = [0, 2\pi]^3\, m^3$. Define $\psi = \sin kx \sin ly \sin mz$ with k, l and m positive integers.

Let the exact solution be,

$$E_1 = \alpha_1 \partial_x \psi, \quad E_2 = \alpha_2 \partial_y \psi, \quad E_3 = \alpha_3 \partial_z \psi$$

The domain Ω is split into two parts, Ω_1 with $z < \pi$ and Ω_2 for $z > \pi$, so that Ω is the union of their closure. The conductivity $\sigma = \sigma_0 + \sigma_1 (x+1)(y+2)(z-\pi)^2$ in Ω_1, and $\sigma = \sigma_0$ in Ω_2. Set $\epsilon_r = 0, \mu_r = 1$ and $\omega = 10^6$Hz. The other parameters are chosen as to be $\alpha_1 = \alpha_2 = -2\text{V}, \alpha_3 = 1\text{V}, k = l = m = 1, \sigma_0 = 10\text{S/m}$ and $\sigma_1 = 1\text{S/m}$. Note that ψ is based on sine functions, causing the tangential electricfield components to vanish at the boundaries in agreement with the PEC boundary conditions used here. The current source is defined by $\mathbf{J}_s = -\tilde{\sigma}\hat{\mathbf{E}} + \nabla \times (i\omega\mu)^{-1} \nabla \times \mathbf{E}$. Using the exact solution this results in:

$$\begin{aligned} \mathbf{J}_s &= -\tilde{\sigma} \begin{pmatrix} \alpha_1 \partial_x \psi \\ \alpha_2 \partial_y \psi \\ \alpha_3 \partial_z \psi \end{pmatrix} + \\ & (i\omega\mu)^{-1} \begin{pmatrix} \left[l^2(\alpha_1 - \alpha_2) + m^2(\alpha_1 - \alpha_3)\right] \partial_x \psi \\ \left[k^2(\alpha_2 - \alpha_1) + m^2(\alpha_2 - \alpha_3)\right] \partial_y \psi \\ \left[k^2(\alpha_3 - \alpha_1) + l^2(\alpha_3 - \alpha_2)\right] \partial_z \psi \end{pmatrix} \end{aligned}$$

Next section a short description of grid-stretching is given. In the last section of this chapter a list can be found of the several tests and problems encountered by using the multigridsolver to solve this testproblem.

7.1.1 Grid stretching

The grid stretching used by Mulder is called power law grid stretching. For instance, assume there are $N_x = N_y = N_z = 2^m + 1$ gridpoints in each direction. One option can be a equidistant grid with spatial mesh size h. However, suppose there is a small, compact area like a sphere were many discontinuities occur in the parameters of the equation which lives on whole domain. Furthermore, from a particular distance from this area there are no problems with the parameters anymore. On an equidistant every the spatial mesh size is the same. Because it would be very expensive to refine the whole grid, it would be very useful to have more fine gridcells only in the sphere and to keep the number of gridpoints the same. The solution is grid stretching.

The idea behind stretching is to make the cells around the origin very small and let the spatial mesh size increase for each cell that lays further from this origin. The spatial mesh ratio between two arbitrary neighboring cells is the same, $1 + \alpha$. Obviously, this is called power law stretching as the spatial mesh size satisfies the following formula:

$$h_i(j) = h_i(0)(1 + \alpha)^j$$

Where $h_i(j)$ is the spatial mesh size of cell j in direction $i = x, y, z$. And $h_i(0)$ is the spatial mesh size of the first grid cell lying at the origin.

An example of a grid stretched from the source:

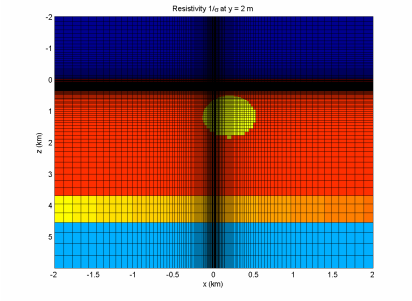

7.2 Problems encountered (test) cases

In this section a list of problems and there possible causes encountered solving these problems with the multigridsolver described above.

1. Consider the testproblem based on eigenvalues (section ??). Let $\sigma_0 = 10\text{S/m}$ and $\sigma_1 = 1\text{S/m}$ which avoids zero values for the conductivity.

N	$h_{\max}$	MG	bi	$l_2/h^2_{\max}$	$l_{\max}/h^2_{\max}$
16	0.39	7	6	2.0	0.41
32	0.20	8	7	2.0	0.48
64	0.098	8	7	2.1	0.49
128	0.049	8	6	2.1	0.49

(Table 1)

The table above lists the number of iterations and errors. The number of gridcells in each direction is given by $N_x = N_y = N_z = N$. For each grid, the number of iterations with pure multigrid (MG) and with multigrid as a preconditioner for BiCGstab (bi) is given. Note that BiCGstab costs a bit more per iteration because it requires an additional evaluation of the residual. Also, each BiCGstab is counted two iterations because it involves two multigrid cycles. Because convergence checks are carried out halfway and at the end of a full iteration step, the method may stop after an odd number of iterations. The iterations were stopped when the l_2 norm (see Appendix ??) of the residual had dropped a factor 10^{-8} from it's original value for a zero solution. The error in the numerical solution is listed in various norms. Here $l_{\max}$ (see Appendix ??) is the maximum difference with the exact solution. For the exact solution the point-values at the edge midpoints have been used.
The results in the table above show grid independent convergence for the multigrid method. The number of iterations of BiCGstab is one less but not worth the extra cost in terms of CPU time. The errors confirm the second order accuracy of the solution. They have been divided by the square of the largest spatial mesh size $h_{\max} = \max\{h^x_k, h^y_l, h^z_m\}$.

2. Again, consider the testproblem based on eigenvalues. Let $\sigma_0 = 10\text{S/m}$ and $\sigma_1 = 1\text{S/m}$ and use power law grid stretching with a spatial mesh size ratio $(1 + \alpha)$ between two neighboring cells. Let $\alpha = 0.04$.

N	$h_{\max}$	MG	bi	$l_2/h^2_{\max}$	$l_{\max}/h^2_{\max}$
16	0.45	8	6	1.9	0.36
32	0.26	11	8	1.9	0.33
64	0.17	12	14	1.7	0.29
128	0.13	81	32	1.6	0.28

The grid independent convergence rates of Multgrid are lost. However, the BICG-method is able to deal with the slow converging components of the solution and needs significant less iterations to converge. Again the errors confirm second order accuracy.

In the article of Mulder 'a multigrid solver for 3-D electromagnetic diffusion' several more test were carried out. Of course with different values for σ_0 and σ_1, also a minimum-norm solution is constructed when a vacuum region appears. As to be expected, grid stretching causes more trouble. For some parameter settings the multigrid method does not converge any more. The iterations were stopped when the norm of the residual did not decrease. Even BiCGstab did not converge in less than 100 iterations in that particular situation.

Also more 'realistic ' testcases can be found in the article of Mulder. All cases show the same pattern. Without grid stretching the method converges usually, but when the power law ratio α becomes significant large (> 0.02) Multigrid breaks down or needs a very large number of iterations to converge. It can be said that stretching the grid has an effect similar to the use of variable coefficients, in this case $\mu_r^{-1}(\mathbf{x})$, inside the difference operators. When these coefficients show large variations or the grid is stretched the problem becomes anisotropic. This will become more clear next chapter.

8 Anisotropy

As become clear in the previous section, anisotropy in the Maxwell equations through grid stretching is the biggest problem in the deterioration of the convergence rates of the multigridsolver. In the chapter concerning multigrid there is mentioned earlier that anisotropy could be a possible troublemaker. In this chapter a definition of anisotropy is given and afterwards how grid stretching could cause this effect.

8.1 Definition

The Maxwell equations were stated in 3D. But to get a clear view of the definition of anisotropy it is easier to give a 2D simple example. The extension

from 2D to 3D, which will not be done here, is quite trivial because the basic principles of anisotropy in 2D and 3D are the same. However, the problem is a bit more complex in 3D because there are simply more possibilities to adapt the multigridcomponents to solve the problem of anisotropy.

So, the Maxwellequations are temporarily not important and a 2D anisotropic elliptic equation is introduced:

$$\begin{aligned} -\varepsilon\partial_{xx}u - \partial_{yy}u &= f^{\Omega}(x,y), \quad \left(\Omega = (0,1)^2, \quad u = u(x,y)\right) \\ u &= f^{\Gamma}(x,y), \quad (\partial\Omega) \end{aligned} \tag{6}$$

Here $0 < \varepsilon << 1$, the case were $\varepsilon >> 1$ is not any different but than the role of the directions x and y interchange.

Discretize equation (6) with a standard 5-point difference operator, then the following discrete problem is obtained:

$$\begin{aligned} A_h(\varepsilon)u_h &= f_h^{\Omega}, \quad (\Omega_h) \\ u_h &= f^{\Gamma}, \quad (\Gamma_h) \end{aligned}$$

where Ω_h is a square grid with spatial mesh size $h = h_x = h_y$ (similar as in figure (4)) and Γ_h is the set of gridpoints lying on the boundary of Ω. In stencil notation, the discrete operator $A_h(\varepsilon)$:

$$A_h(\varepsilon) = \frac{1}{h^2}\begin{bmatrix} & -1 & \\ -\varepsilon & 2(1+\varepsilon) & -\varepsilon \\ & -1 & \end{bmatrix}_h$$

In this case, the discrete anisotropy is aligned with the grid. In 2D such problems are characterized by the coefficients in fornt of the u_{xx} and u_{yy} terms, which may differ by orders of magnitude. In next section the role of anisotropy introduced by discretization will be discussed. Indeed this is the case with stretched grids.

So far, nothing seems wrong with the discrete oprator $A_h(\varepsilon)$. However, if ε goes to 0, the $h-$ellipticity (uitleg!!) measure of the anisotropic operator tends to 0. Soon it will become clear that the smoothing properties of a standard pointwise smoothing scheme will deteriorate for $\varepsilon \to 0$. Suppose that a standard pointwise relaxation such as Gauss-Seidel in lexicographical order (GS-LEX) is applied to system above. Then it will appear that the smoothing effect of the error is very ppor with respect to the x-direction. The reason is that pointwise relaxation has a smoothing effect only with respect to the "strong coupling " in the operator, i.e. the y-direction. If the error is plotted after several iteration steps, the error will be smooth in y-direction and capricious in the x-direction.

For example, consider GS-LEX, then the error relation becomes:

$$e_h^{m+1}(x_k, y_l) = \frac{1}{2(\varepsilon+1)}[\varepsilon e_h^{m+1}(x_{k-1}, y_l) + \varepsilon e_h^m(x_{k+1}, y_l) + e_h^{m+1}(x_k, y_{l-1}) + e_h^m(x_k, y_{l+1})]$$

Now let $\varepsilon \to 0$,

$$e_h^{m+1}(x_k, y_l) = \frac{1}{2}[e_h^{m+1}(x_k, y_{l-1}) + e_h^m(x_k, y_{l+1})]$$

Obviously, there is no averaging effect with respect to the x-direction and therefore no smoothing with respect to this direction is achieved. Such non smooth erros can no longer by efficiently reduced by means of a coarser grid which is obtained by standard coarsening, thus by doubling the mesh size in both directions.

This failure can be explained by applying LFA smoothing analysis (Oosterlee, ???) to the GS-LEX smoother for the problem. The multigrid convergence factor will increase towards 1 for $\varepsilon \to 0$ or $\varepsilon \to \infty$. In general, pointwise relaxation and standard coarsening is not a reasonable combination for highly anisotropic problems.

Next chapter will provide solutions for these complications.

8.2 Anisotropy on stretched grid

As said above, when stretched grids are used, the discretization may introduce anisotropies. Consider a standard 2D Poisson like elliptic-equation:

$$\begin{aligned} -\partial_{xx}u - \partial_{yy}u &= f^{\Omega}(x,y), \quad \left(\Omega = (0,1)^2, \quad u = u(x,y)\right) \\ u &= f^{\Gamma}(x,y), \quad (\partial\Omega) \end{aligned} \tag{7}$$

Introduce the following, stretched, grid:

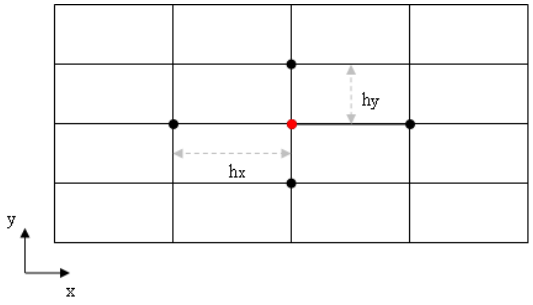

Where, $h_x = \frac{h_y}{\sqrt{\varepsilon}}$ with $0 < \varepsilon < 1$. Use standard central differences for discretization with $h_y = h$:

$$\partial_{xx}u \simeq \varepsilon\frac{u(x_{k-1},y_l)-2u(x_k,y_l)+u(x_{k+1},y_l)}{h^2}+O(h^2)$$
$$\partial_{yy}u \simeq \frac{u(x_k,y_{l-1})-2u(x_k,y_l)+u(x_k,y_{l+1})}{h^2}+O(h^2)$$

Obviously, the same discrete operator as for equation (6) is obtained.

A similar procedure can be followed with more complex stretched grid, e.g. as used in the testproblem above (power law grid stretching), however the idea behind the anisotropy remains the same.

9 Solving anisotropy

In this chapter two possible solutions for the problems encountered with the multigridsolver caused by anisotropy in the Maxwell equations are given. As a lot research has been done on the problem of anisotropy, it is to be expected that both remedies will improve the multigridsolver. However, keep in mind that this is just a research proposal, maybe more advanced tools have to be applied to get a better performance of the multigridsolver. These techniques will not be introduced yet.

According to "Multigrid solution methods and parallelization for computational science applications " by Oosterlee et al (??) the use of semi coarsening and linesmoothers will improve the multigrid performance.

9.1 Semi coarsening

Again, consider the example of the 2D elliptic equation (7) with anisotropy due to grid stretching. The idea is to keep pointwise relaxation for smoothing but to change the grid coarsening according to the one-dimensional smoothness of errors. This means that a coarser grid is defined by doubling the mesh size only in that direction in which the errors are smooth:

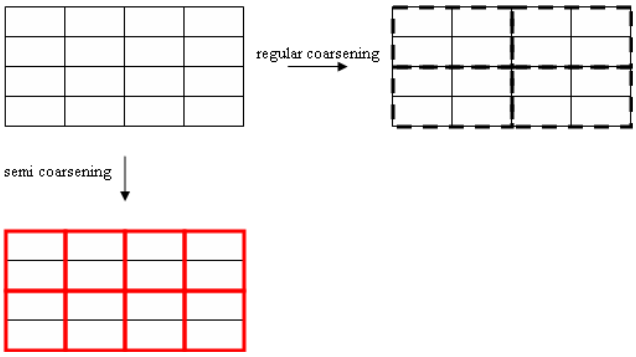

Suppose regular (normal) coarsening has been used. After one gridcoarsening, the grid goes from 4x4 cells to 2x2 cells. But, the stretched cells are still

intact and this yields an anisotropic discrete operator for equation (7). Now apply semi coarsening. After one gridcoarsening, the grid goes from 4x4 cells to 4x2 gridcells. It is easy to see that the grid cells are, in this particular case, not rectangles but squares. Hence, $H_x = H_y$ and the anisotropy at this coarser grid will not be dominating in the discretization of the equation (7). It can be shown by LFA analysis of the error that the quality of a smoother depends on the range of high frequencies and thus on the choice of the coarse grid.

One remark has to be made. Of course there are practical complication with the use of semi coarsening. The restriction and prolongation operators have to be adapted to work on the coarser grids also. It is obvious that full weighting and linear, bilinear interpolation as described above (Multigrid Components Mulder, ??) use different electricfield components to compute coarse-grid electricfield components when the structure of the grid changes.

9.2 Linesmoother

The other approach is the use of a linesmoother. The idea is to keep standard multigrid coarsening, but to change the relaxation procedure from pointwise relaxation to linewise relaxation. This means that all unknowns on one line are updated simultaneously. A linesmoother in x-direction will update all the unknowns lying on a line $[x_1, x_{Nx}]$ with y_l arbitrary and constant. For y (and in 3D z) this will be straightforward.

Gauss-Seidel-type line relaxations are particularly efficient smoother for anisotropic problems (if the anisotropy is aligned with the grid). This is due to the general observation that errors become smooth in both directions if strongly connected unknowns are updated collectively. In case of grid stretching this is of course the case. Suppose grid stretching only in x-direction as in Anisotropy on stretched grid (section ??). Obvious, there is a strong coupling between the unknowns in x-direction due to the big differences between h_y and h_x.

In Oosterlee et al (??) LFA analysis is applied to a lexicographic line Gauss-Seidel smoother. The use of such a smoother decreases the anisotropy significantly. There are, of course, other line smoothers one can use, e.g. ω-Jacobi or zebra line Gauss-Seidel smoothing (line smoother x-direction, first all even rows in y-direction and next the odd rows). However, Mulder uses a pointwise symmetric GS-LEX and therefore it is to be expected that a GS-LEX linesmoother will give improvement on the performance of the Multigridsolver.

10 Research proposal

Wim Mulder of Shell International Exploration and Production has developed a multigridsolver in order to solve the time-harmonic Maxwell equations. These equations are coming from a 3D EM diffusion method which is used in the exploration and investigation of possible oil/gas reservoirs in the (sea) surface (??).

For small scale (test) problems the multigridsolver shows no performance leak. However, when the gridsize increases and (power law) grid stretching has been applied, the discretization of the Maxwell equations become anisotropic in all three directions. There are several possible solutions for this problem. First, the research will focus on two improvements of the multigridsolver. Semi coarsening and linesmoothing and of course the combination of these two mathematical tools.

In order to test these improvements a testproblem is used which is developed by Mulder and based on a testproblem that can be found in Aruliah et al (2001). The idea behind this problem is to express the solution of the Maxwell equation in eigenfunctions.

Matlabcode is already provided by Mulder and has to be adapted to make it more suitable for further adaptations of the components of the multigridsolver. When the testproblem provides satisfactory results the improvements will be implemented in more realistic problems and fine-tuning of these new components will be necessary. Also, more analysis has to be done concerning the who and why of the (possible) improvements of the solver. LFA and Fourier analysis can be used.

At the end of this research, hopefully an improved multigrid solver can be presented with a sound mathematical foundation.

11 References

References

[1] Mulder, W.A. A multigrid solver for 3D electromagnetic diffusion

[2] (Hier ook bronnen Wim???)

[3] Oosterlee, C.W., Trottenberg U„ Schüller A. Multigrid solution methods and Parallelization for Computational Science Applications

[4] Aruliah, D.A. PhD Thesis (Naam?)

[5] Hiptmair R. Multigrid method for Maxwell equations

[6] Unsworth, M. New developments in conventional hydrocarbon exploration with electromagnetic methods

12 Appendix

* Code aangepaste multigridsolver zonder semicoarsening en linesmoother
  * Voorlopig de kopieen van:
    - Recursie overzicht F-cycle
    - De pointsmoother uitgeschreven
    - Overzicht F-cycle
  * Matlab code functie overzicht